Smart Mater. Struct. **22** (2013) 025036 (10pp) doi:10.1088/0964-1726/22/2/025036

Energy harvesting from hydraulic pressure fluctuations

K A Cunefare, E A Skow, A Erturk, J Savor, N Verma and M R Cacan

G W Woodruff School of Mechanical Engineering, Georgia Institute of Technology, Atlanta, GA 30332-0405, USA

E-mail: eskow3@gatech.edu

Received 22 August 2012, in final form 19 November 2012
Published 29 January 2013
Online at stacks.iop.org/SMS/22/025036

Abstract
State-of-the-art hydraulic hose and piping systems employ integral sensor nodes for structural health monitoring to avoid catastrophic failures. Energy harvesting in hydraulic systems could enable self-powered wireless sensor nodes for applications such as energy-autonomous structural health monitoring and prognosis. Hydraulic systems inherently have a high energy intensity associated with the mean pressure and flow. Accompanying the mean pressure is the dynamic pressure ripple, which is caused by the action of pumps and actuators. Pressure ripple is a deterministic source with a periodic time-domain behavior conducive to energy harvesting. An energy harvester prototype was designed for generating low-power electricity from pressure ripples. The prototype employed an axially-poled off-the-shelf piezoelectric stack. A housing isolated the stack from the hydraulic fluid while maintaining a mechanical coupling allowing for dynamic-pressure-induced deflection of the stack. The prototype exhibited an off-resonance energy harvesting problem since the fundamental resonance of the piezoelectric stack was much higher than the frequency content of the pressure ripple. The prototype was designed to provide a suitable power output for powering sensors with a maximum output of 1.2 mW. This work also presents electromechanical model simulations and experimental characterization of the piezoelectric power output from the pressure ripple in terms of the force transmitted into the harvester.

(Some figures may appear in colour only in the online journal)

1. Introduction

The harvesting of ambient energy for powering small electronic components has been heavily researched in the last decade [1–4]. The main goal in this research field is to enable self-powered wireless electronic systems. In this way, the maintenance requirements for battery replacement as well as the chemical waste of conventional batteries can be reduced. Most of the existing research on energy harvesting has focused on the direct conversion of vibrations into electricity [1]. Flow-excited power generators covered in the existing literature are mainly focused on (1) converting flow-induced aeroelastic or hydroelastic vibrations into electricity or (2) implementing Helmholtz resonators and sonic crystals for indirect use of flow pressure (mostly air flow), by creating vibrations of the generator system. The generator system is typically a piezoelectric beam or membrane, an electroactive polymer, or an inductive coil and magnet arrangement.

Other than the efforts toward miniaturizing the classical wind turbine design [5–8] in conjunction with fan rotors and DC motors, researchers have become interested in exploiting aeroelastic/hydroelastic and acoustic phenomena for flow energy harvesting by means of electromechanical transducers. The first use of a piezoelectric interface in flow energy harvesting appears to be the bluff body—a PVDF (polyvinylidene fluoride) membrane configuration known as the ‘energy harvesting eel’—tested under water by Allen and Smits [9]. The von Kármán vortex street formed behind the bluff body excites the piezoelectric PVDF to extract electricity from flow-induced vibrations through the piezoelectric effect. Unlike piezoelectric ceramics, PVDF films are very weakly coupled (in terms of their piezoelectric constants) to generate usable electricity, but they are very

compliant, such that they may undergo large deformations at low frequencies. Vortex-induced oscillations of piezoelectric cantilevers (PZT-based ceramic and/or PVDF) located behind bluff bodies (variants and extensions of the configuration introduced by Allen and Smits [9]) were also investigated by Pobering and Schwesinger [10] and Akaydin *et al* [11] through experiments and numerical simulations.

For the piezoaeroelastic problem of energy harvesting from airflow excitation of a cantilevered plate with embedded piezoceramics, De Marqui *et al* [12, 13] presented finite-element models based on the vortex-lattice method [12] and the doublet-lattice method [13] of aeroelasticity. Time-domain simulations [12] were given for a cantilevered plate with embedded piezoceramics for various airflow speeds below the linear flutter speed and at the flutter boundary. Frequency-domain simulations [13] considering resistive and resistive–inductive circuits were also presented focusing on the linear response at the flutter boundary. Bryant *et al* [14, 15] studied the aeroelastic energy harvesting problem for a typical section by using a finite state theory. Erturk *et al* [16] presented an experimentally validated lumped-parameter model for an airfoil with piezoceramics attached to plunge stiffness members using Theodorsen's unsteady aerodynamic model. Piezoelectric power generation at the flutter boundary and the minor shift in the linear flutter speed were also discussed. More recently, the nonlinear version of the same setup with a free play in the pitch degree of freedom has been investigated for reducing the cut-in speed of limit-cycle oscillations (LCO) [17]. An extensive analysis of the energy harvesting potential for a foil-damper system was presented by Peng and Zhu [18] using a Navier–Stokes model without focusing on a specific transduction mechanism.

As an alternative to airfoil-based and cantilevered wing-based configurations, Clair *et al* [19] presented a 'harmonica-inspired' design that uses a piezoelectric beam embedded within a cavity under airflow from a pressurized chamber. A shear-mode piezoelectric energy harvester operated under pressurized water flow was presented by Wang and Liu [20] by combining a pressure chamber with a flexible diaphragm and piezoelectric film configuration. Deterre *et al* [21] provided a model and preliminary tests for fluidic pressure energy harvesting through the deflection of a piezoelectric diaphragm for use in low mean pressure environments, such as implantable medical devices exposed to pressure from blood. Both Wang *et al* and Deterre *et al* utilize a flexible piezoelectric diaphragm (with a thickness of less than 300 μm) in combination with a pressure chamber to induce bending vibrations in the piezoelectric to generate power. Elvin and Elvin [22] theoretically investigated the flutter response of a cantilevered pipe with piezoceramic patches for power generation from liquid flow and its effect on the flutter instability. Tang *et al* [23] presented a rigorous analysis of the energy transfer from the fluid to the structure for self-excited vibrations due to axial flow over a cantilever. Piezoelectric energy harvesting from LCO under axial flow over a cantilever beam has also been discussed by Dunnmon *et al* [24] recently. Kwon [25] considered a T-shaped cantilever beam that causes vortex street formation over the cantilever in response to axial flow (with the cut-in speed of 4 m s^{-1}). Giacomello and Porfiri [26] investigated underwater flapping of an ionic polymer-metal composite (IPMC) flag. Recent efforts have also employed electromagnetic induction for converting aeroelastic vibrations into electricity through flutter [27], wake galloping [28], and bluff body-based oscillations [29].

Other efforts of harvesting fluidic energy have considered exploiting acoustic phenomena for low-power generation from air-borne waves. Helmholtz resonator-based acoustic energy harvester configurations employing piezoelectric and electromagnetic transductions were introduced by Horowitz *et al* [30] and Kim *et al* [31], respectively. Wu *et al* [32] located a PVDF membrane inside the cavity of a sonic crystal for acoustic energy harvesting.

In this paper, the exploitation of pressure fluctuations in hydraulic systems is investigated for low-power electricity generation through piezoelectric transduction. In a hydraulic system, an energy harvesting technology might be integrated with health-monitoring sensors and eliminate the need for batteries or wires providing power to individual sensors. In the following, a Hydraulic Pressure Energy Harvester (HPEH) prototype is introduced for converting pressure ripple into electricity by using a piezoelectric stack arrangement. The piezoelectric stack is installed into the hydraulic system to directly allow the pressure fluctuations in the system to deflect the stack, which generates more than the estimated needed power of 70 μW for target applications. The high power intensity of hydraulic systems allows for deflections of the piezoelectric stack to occur and for target power values to be exceeded despite off-resonance piezoelectric stack excitation. Details of the testing procedure and performance results are presented for various static and dynamic pressure levels. A lumped-parameter electromechanical model is also described and validated to predict the electrical power output in terms of the hydraulic pressure ripple.

2. Power intensity of pressure ripple in hydraulic systems

The energy harvester introduced in the following sections utilizes periodic pressure disturbances within a hydraulic system, termed dynamic pressure, to create non-negligible electrical power. The high power intensity of hydraulic systems provides suitable grounds for using the piezoelectric effect to produce power through the exploitation of the pressure ripple of the system. It is useful to review the relationship between the fluidic power intensity and dynamic pressure to quantify the level of energy input to the harvester.

In a hydraulic system with pressure fluctuations, the power intensity I is described by

$$I = \frac{P^2}{2\rho c} \tag{1}$$

where c is the speed of sound in the hydraulic fluid, $\sim$1400 m s^{-1}, ρ is the density of hydraulic fluid, $\sim$800 kg m^{-3}, and P is the amplitude of the dynamic pressure in Pa. Measurement of the pressure ripple then

allows for the intensity to be calculated. Pressure ripple in the hydraulics community represents the peak-to-peak amplitude of the dynamic pressure. For example, if a hydraulic system has a dynamic pressure amplitude of 100 kPa, which is a relatively low level in hydraulic systems, the intensity level is 450 mW cm^{-2}. In comparison, airborne acoustic noise has an intensity level of 0.96 μW cm^{-2} from a relatively high sound pressure level of 100 dB (ref 20 μPa). In addition, the magnitude of the pressure ripple typically increases with the mean, or static, pressure of a hydraulic system. Through the comparison presented and the increase of the power intensity when increasing the mean pressure, it is evident that pressure ripple in hydraulic systems represents a significantly high-energy-intensity source as compared to other sources. With a large power intensity available in a hydraulic system, it is possible to use a HPEH to convert hydraulic pressure energy into electrical power without affecting the hydraulic system. Additionally, the high energy density allows this system to perform off-resonance of the piezoelectric stack which is uncommon for energy harvesting systems. This can allow electrical power from HPEHs to replace batteries or external power supplies for structural health-monitoring sensors applied to hydraulic systems.

3. Modeling of power generation using a piezoelectric stack

To facilitate effective designs and testing parameters for HPEH devices, an analytic, linear model has been implemented to understand the piezoelectric stack interactions with a periodic pressure ripple. Electromechanical modeling details of deterministic and stochastic energy harvesting from piezoelectric stacks under direct force excitation can be found in Zhao and Erturk [33]. A piezoelectric stack, formed from multiple layers of piezoelectric layers, is forced by pressure ripples traveling through hydraulic lines. This causes physical deflections of the piezoelectric material and produces a voltage potential across the electrodes as a result of the direct piezoelectric effect. The electrode terminals are connected to an external resistive load to complete an electric circuit. For an arbitrary force input transmitted to the stack, the governing linear electromechanical equation for AC power generation is given by [33]

$$C_{\mathrm{p}}\frac{\mathrm{d}v(t)}{\mathrm{d}t}+\frac{v(t)}{R_{\mathrm{l}}}=d_{33}^{\mathrm{eff}}\frac{\mathrm{d}F(t)}{\mathrm{d}t} \tag{2}$$

where C_{p} is the capacitance of the piezoelectric stack at constant stress, $v(t)$ is the voltage across the electrode terminals, $F(t)$ is the dynamic axial force transmitted to the stack, d_{33}^{eff} is the effective piezoelectric strain constant, and R_{l} is the load resistance. The fundamental assumption made in deriving equation (2) is that the highest significant frequency content of the dynamic force input $F(t)$ is much lower than the fundamental resonance frequency of the piezoelectric stack. This characteristic property of the hydraulic environment results in an inability for the piezoelectric stack to be excited at resonance, unlike typical vibration-based energy harvesters designed for resonant excitation to use bending vibrations [1–4]. For harmonic excitation of the form $F(t)=F_0\mathrm{e}^{\mathrm{j}\omega t}$, where F_0 is the force amplitude, ω is the radial excitation frequency, and j is the unit imaginary number, the steady-state voltage across the resistive load is [33]

$$v(t)=\mathrm{j}\omega d_{33}^{\mathrm{eff}}\left(\mathrm{j}\omega C_{\mathrm{p}}+\frac{1}{R_{\mathrm{l}}}\right)^{-1}F_0\mathrm{e}^{\mathrm{j}\omega t}. \tag{3}$$

Hence, in the presence of a single frequency component, or dominant frequency component, the peak power at steady state is

$$\Pi=\left|\frac{v^2(t)}{R_{\mathrm{l}}}\right|=\frac{R_{\mathrm{l}}}{1+\omega^2R_{\mathrm{l}}^2C_{\mathrm{p}}^2}(\omega d_{33}^{\mathrm{eff}}F_0)^2 \tag{4}$$

which can be used to find the optimal electrical load for maximum peak power as

$$\left.\frac{\partial\Pi}{\partial R_{\mathrm{l}}}\right|_{R_{\mathrm{l}}=R_{\mathrm{l}}^{\mathrm{opt}}}=0\rightarrow R_{\mathrm{l}}^{\mathrm{opt}}=\frac{1}{\omega C_{\mathrm{p}}}. \tag{5}$$

The peak power output for the optimal load is then

$$\Pi_{\mathrm{max}}=\Pi|_{R_{\mathrm{l}}=R_{\mathrm{l}}^{\mathrm{opt}}}=\frac{\omega(d_{33}^{\mathrm{eff}}F_0)^2}{2C_{\mathrm{p}}}. \tag{6}$$

Under harmonic excitation, the average power for an arbitrary load resistance is therefore obtained from equation (4) and by using F_{RMS}, where $F_{\mathrm{RMS}}=F_0/\sqrt{2}$. Hence, average power is $\Pi_{\mathrm{ave}}=\Pi/2$, which takes its maximum value of $\Pi_{\mathrm{max}}^{\mathrm{ave}}=\Pi_{\mathrm{max}}/2$ for an electrical load of $R_{\mathrm{l}}^{\mathrm{opt}}=1/\omega C_{\mathrm{p}}$.

While the harmonic representation is useful for simpler system inputs and determination of unknown quantities, hydraulic systems employed for energy harvesting have periodic force inputs, for which the derivation follows. From equation (3), one can define the voltage output–to–force input frequency response function (FRF), $\alpha(\omega)$, for an arbitrary electrical resistance as

$$\alpha(\omega)=\frac{v(t)}{F_0\mathrm{e}^{\mathrm{j}\omega t}}=\mathrm{j}\omega d_{33}^{\mathrm{eff}}\left(\mathrm{j}\omega C_{\mathrm{p}}+\frac{1}{R_{\mathrm{l}}}\right)^{-1}. \tag{7}$$

If the force transmitted to the stack is a periodic function of the form $F(t)=F(t+T)$, where T is the periodic fluctuation, then its Fourier series representation and equation (7) can be used to estimate the periodic voltage output $v(t)$ for a given resistive load [34]. It should be noted that the periodic function $F(t)$ is such that the highest harmonic of its Fourier expansion is much lower than the fundamental resonance of the piezoelectric stack so that the frequency response expression used in the Fourier series-based solution is valid. The foregoing linear derivation also assumes that the static component of the force may alter only the capacitance, which can easily be accounted for by using the capacitance value measured under the respective static pressure.

Since the force transmitted to the piezoelectric stack is acting on the stack's cross-sectional area, A, i.e., $F_0=P_0A$ (where P_0 is the transmitted pressure amplitude), then, equation (3) can be rewritten as

$$v(t)=\mathrm{j}\omega d_{33}^{\mathrm{eff}}\left(\mathrm{j}\omega C_{\mathrm{p}}+\frac{1}{R_{\mathrm{l}}}\right)^{-1}AP_0\mathrm{e}^{\mathrm{j}\omega t} \tag{8}$$

which leads to equation (6) becoming

$$\Pi_{\max} = \Pi|_{R_l=R_l^{\text{opt}}} = \frac{\omega(d_{33}^{\text{eff}} A P_0)^2}{2C_p} \tag{9}$$

where it is evident that the maximum power output will vary with the square of the dynamic pressure, $\Pi_{\max} \propto P_0^2$.

Power output corresponds to dynamic pressure ripple; however, static pressure values will be referenced in order to quantitatively distinguish between the low and high pressure ripple tests presented later. Static pressure values relate to HPEH system power output levels because they induce larger pressure amplitudes in the hydraulic system, yet using identical static pressure values in different hydraulic systems does not necessarily yield identical pressure ripple values. For this reason, power output comparisons must use power normalized by the input dynamic pressure amplitude or use power produced by identical hydraulic systems. Note that average power is calculated from

$$\Pi_{\text{avg}} = \frac{v_{\text{RMS}}^2}{R_l}, \tag{10}$$

where v_{RMS} is the root-mean-square voltage produced by the harvester. Also, power normalized by pressure is calculated from

$$\Pi_{\text{norm,P}} = \frac{\Pi_{\text{avg}}}{P_{0,\text{RMS}}^2}, \tag{11}$$

which is derived from equations (4) and (9), where $P_{0,\text{RMS}}^2$ is the squared root-mean-square value of the pressure ripple.

The above model represents the interaction of a piezoelectric stack with fluid pressure ripples, however a representation of the interaction of a HPEH device with hydraulic pressure ripples must allow for the fluid-mechanical coupling between the hydraulic fluid and piezoelectric stack. A HPEH device, depicted in figure 1, includes a piezoelectric stack within a housing connected to the hydraulic system with an interface separating the hydraulic fluid from the piezoelectric stack. The interface represents the fluid-mechanical coupling between the piezoelectric stack and pressure ripple. In the case of HPEH systems, the pressure amplitude acts on the fluid-to-stack interface design, causing the force transmitted to the stack to be better represented by $F_0 = P_0 A^{\text{eff}}$, where A^{eff} is the effective area induced by the coupling between the pressure ripple and the stack surface area.

If using a given periodic pressure ripple input, the force to the stack can be amplified through interface modification to increase the effective area. The ratio of the designed area interface of a HPEH device to the cross-sectional area of the piezoelectric stack, referred to as area ratio γ, is used as a design parameter to increase the power output of a device. Currently, effective area can only be determined through the comparison of the predicted power outputs using the stack area and the experimentally obtained power outputs, therefore design parameters and effective parameters differ. Explanation for how this is calculated is discussed in the context for which it is necessary. When comparing HPEH device effective areas, the term effective area ratio, γ_e, is used.

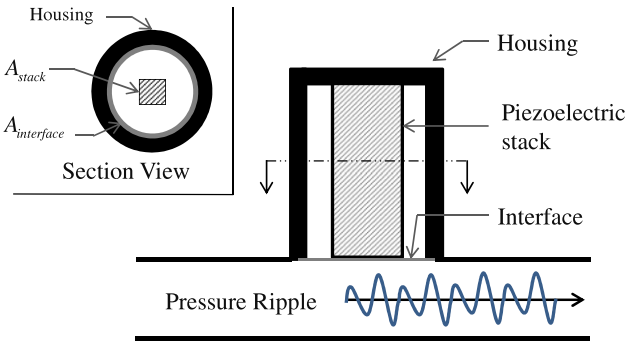

Figure 1. Hydraulic pressure energy harvester schematic.

Two HPEH prototypes were designed and fabricated to exploit the aspects of the model. The first prototype, HPEH1-1, was designed to explore the electromechanical portion of the model. The second prototype, HPEH1-2, explores the fluid-mechanical interface, specifically regarding investigation of the area ratio.

4. Testing of HPEH systems

A hydraulic pump system was used to test the HPEH prototypes. Testing involved three distinct phases: an initial test under static load to assess the pressure integrity of the device, a second phase which tested the peak voltage produced, and a third phase which measured the power output versus load resistance. The HPEH system used a soft PZT in the form of a rectangular prism piezoelectric stack with a cross-section of 6.8 mm × 6.8 mm and a length of 30 mm.

An important aspect in the HPEH design was the fluid-mechanical coupling of the piezoelectric surface area and the pressure fluctuation. The interface needs to be flexible to allow for maximum surface deflection (while still protecting the piezoelectric), but stiff enough to prevent failure of the part. The HPEH interface that isolated the stack from the fluid was composed of a 0.0762 mm thick aluminum diaphragm, which allowed the diaphragm stiffness to be much less than the stack stiffness while still protecting the stack. In addition, exploiting the effective areas of a HPEH device for increased power output was of interest. To analyze the area ratio effect, two versions of the prototype were tested with different internal configurations, denoted as HPEH1-1 and HPEH1-2. Interface improvements were applied to HPEH1-2 design by increasing the designed area ratio from 1 to 2.4 allowing more force to be transmitted from the dynamic pressure to the stack. This force amplification was achieved through using a larger diaphragm area than stack area.

The HPEH system was installed on a mounting block, which was incorporated in line with a dead weight tester for phase 1. The HPEH and block were installed in a hydraulic pump system, as can be seen in figure 2, for phase 2 and 3 testing. Key components of the hydraulic pump system are a nine-piston pump operating at 1500 rpm, yielding a fundamental pressure ripple frequency of 225 Hz, and a needle valve for controlling the static pressure.

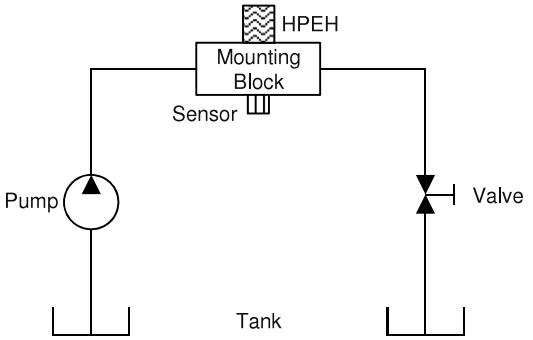

Figure 2. A schematic of the hydraulic pump system used for testing the HPEH in the in-line mounting block for phase 2 and 3 experiments.

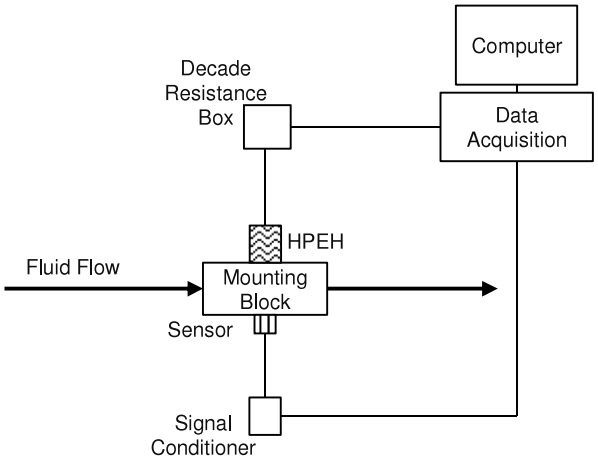

Figure 3. Testing configuration for phase 3, including the sensor and the data acquisition system.

Different mounting blocks are utilized for different procedure phases. For phase 1, the mounting block only allows for the HPEH to be connected to a pressure source, while phase 2 and 3 use a mounting block that includes a connection for a dynamic pressure sensor directly opposite of the HPEH installation location. This ensures the measurement of the dynamic pressure is co-located to that affecting the HPEH.

The first step for testing the HPEH system involved using a hydraulic dead weight tester to ensure the system will meet the static pressure loading for which it was designed to withstand. This includes ensuring that no leaking of hydraulic fluid occurs around the threads into the block or past the fluid-mechanical interface into the internals of the device. After installing the HPEH device and mounting block to the dead weight tester, weights were added in increments that yielded static pressure changes of approximately 0.25 MPa, starting at 2.25 MPa and ending at 3.75 MPa. Additionally, the capacitance of the piezoelectric stack was measured using a multimeter at 2 and 3.5 MPa to provide data to permit the estimation of the optimal resistance value and for better accordance with the model for the two constant stress values tested during phase 3. This test phase allowed for the identification of the statically-loaded capacitance and a simpler troubleshooting process, as fewer parameters were involved.

The second phase of testing was a preliminary voltage response test of the HPEH system. The HPEH was installed on a different mounting block, which includes a dynamic pressure sensor, in line with the hydraulic pump system as depicted in figure 2. The leads to the piezoelectric stack in the HPEH were connected to an oscilloscope through the use of an attenuation probe to measure voltage output of the stack. The pressure sensor was connected to a signal conditioner, which was also connected to the oscilloscope. Once the set-up process was complete, the hydraulic system was turned on with a static pressure of 2.07 MPa, and the voltage signals received were evaluated as to the coupling of the dynamic pressure with the stack output and to ensure voltage level were within phase 3's data acquisition system (DAQ) specifications before proceeding to phase 3. An oscilloscope was used for this test for its ease of use and as a protection buffer for the more complex DAQ used in the next phase.

The final phase of testing was to perform a sweep of resistance values to determine the peak power output of the system. The assembly of the system is the same as phase 2 except with the addition of a resistance load connected in parallel to the HPEH leads. The resistance sweep values depend on the predicted optimal resistance for the stack being tested within the HPEH device. The voltage across the load resistance and the output signal from the dynamic pressure sensor were acquired using a SigLab data acquisition system rather than an oscilloscope; this can be seen in figure 3. The resistance sweep was then performed for static pressure levels of 2.07 $\pm$ 0.03 MPa (300 $\pm$ 5 psi) and 3.45 $\pm$ 0.03 MPa (500$\pm$5 psi). Time- and frequency-domain data were recorded for each test. The data acquisition system was configured for a record length of 8192 points and an anti-aliased bandwidth of 2000 Hz, which provides a frequency resolution of 0.625 Hz.

5. Experimental results and analysis

Both HPEH1-1 and -2 were measured to have a capacitance of 3.06 μF and 3.11 μF when exposed to static pressures of 2 MPa and 3.5 MPa respectively. The peak frequency for the pressure ripple in the hydraulic system was observed to be at 450 Hz, which is the second harmonic of the hydraulic pump system. These values provided for a predicted optimal resistance value, using equation (5), of approximately 115 Ω. Resistor sweep tests were then conducted by varying the load resistance from 10 to 400 Ω to fully characterize the power output around the optimal condition. The power output from HPEH1-1, presented in figure 4, show that the device produced an average maximum power of 153.4 μW (0.052 μW kPa^{-2}) for the root-mean-square pressure ripple amplitude of 54.3 kPa at the low static pressure of 2.07 MPa with a resistance of 130 Ω and 522.4 μW (0.051 μW kPa^{-2}) for the root-mean-square pressure ripple amplitude of 101.4 kPa at the high static pressure level of 3.45 MPa with 110 Ω resistance.

The HPEH time-domain voltage output waveform resembles the dynamic pressure, as seen in figure 5, which

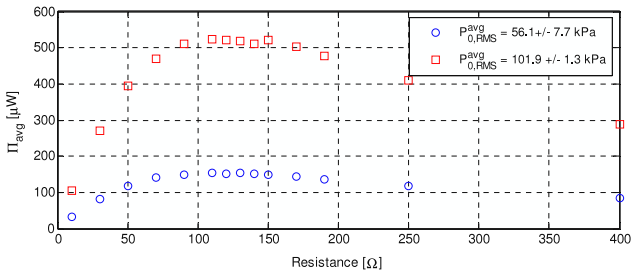

Figure 4. Average power versus resistance for HPEH1-1 at static pressure of 2.07 and 3.45 MPa.

indicates the coupled nature of the dynamic pressure wave and the voltage output by the piezoelectric stack. The spectrum plots in figure 6 show that most of the available energy to be harvested in the hydraulic system occurs at the second harmonic or 450 Hz, which corresponds to the maximum pressure magnitude and stack voltage magnitude.

As can be seen in figure 4, the higher pressure ripple amplitude and accurate impedance matching make a significant difference in the power output. The higher static pressure load yields a higher pressure ripple, as seen in figures 5 and 6, to excite the stack allowing for higher power outputs. It should be noted that small deviations in the power plot are a result of static pressure adjustment between tests in order to maintain constant mean pressure. This was necessitated by the heating of the hydraulic fluid over the duration of the experiments, leading to drift in the static pressure, and due to the low resolution of the static load pressure gauge (±0.03 MPa) that was used in manually setting the static pressure. Regarding impedance matching, resistance values at peak power match well to the predicted optimal resistance discussed earlier. For the given pump and stack used, the optimal resistance value was found to be 115 Ω via equation (5), which is within the range of 110–130 Ω where maximum power output was observed for this system. The testing parameters used provide guidelines for future HPEH designs and for resistance sweeps on different HPEH systems. Results from these tests are summarized in table 1.

As indicated by equation (9), an increase of pressure ripple or effective area will cause the power output of the HPEH device to increase when using the same piezoelectric stack; this implication was investigated in the second version of the HPEH prototype (HPEH1-2). With the increased area ratio in the HPEH1-2 design, twice the power output per squared pressure amplitude input was produced in comparison to HPEH1-1, as shown in figure 7 and table 1. Time-domain and spectrum plots for HPEH1-2 are not included for brevity as similar results are obtained in comparison to HPEH1-1 plots, excepting that the input pressure amplitude and output stack voltage amplitude are higher, as indicated by the pressure and power results in table 1. Figure 7 shows the power normalized by the squared pressure amplitude to

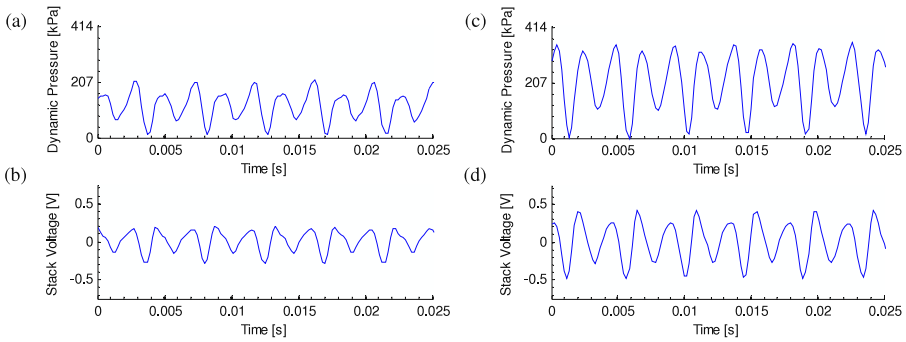

Figure 5. Results of experimental tests on HPEH1-1 for (a), (b) 2.07 MPa and (c), (d) 3.45 MPa showing the dynamic pressure and stack voltage at 120 Ω load resistance.

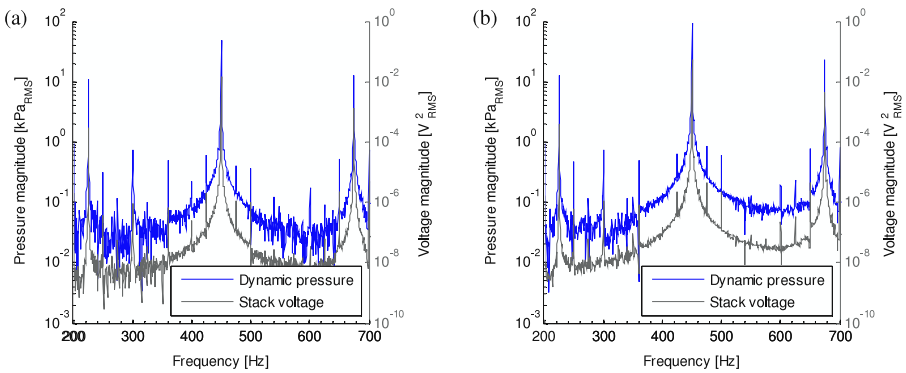

Figure 6. Frequency spectrum from HPEH1-1 for the experiments conducted at (a) 2.07 MPa and (b) 3.45 MPa with 120 Ω load resistance.

Table 1. Experimental results comparing the two different HPEH configurations where the resistance designates the test at which maximum power and respective measurements occurred.

	HPEH1-1		HPEH1-2	
Static pressure, ±0.03 (MPa)	2.07	3.45	2.07	3.45
Maximum average power (μW)	153.4	522.4	383.9	1226
Normalized power (μW kPa^{-2})	0.052	0.051	0.110	0.102
Max. avg. power per volume (μW mm^{-3})	0.111	0.377	0.277	0.884
Pressure amplitude (RMS) (kPa)	54.3	101.4	59.0	109.5
Resistance (Ω)	130	110	130	120

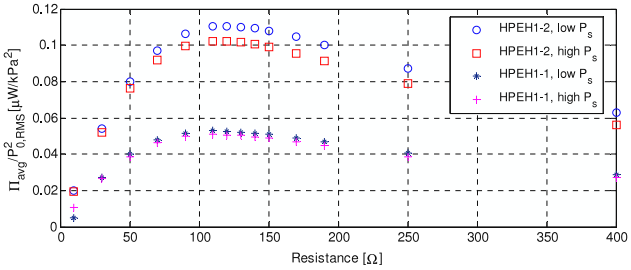

Figure 7. Normalized average power versus resistance for HPEH1-2 and HPEH1-1 at 2.07 and 3.45 MPa (low and high static pressure).

account for the different pressure ripple input to the HPEH systems. With the increased static pressure, the power output efficiency decreased, as seen in figure 7. The doubled power output per squared pressure amplitude demonstrates that increasing the ratio of the dynamic pressure contact area to the piezoelectric cross-sectional area allows for higher power output, however, this increase was lower than expected when considering the designed area ratio value. Hence, a method for determining the effective area of the fluid-mechanical coupling in the HPEH device prior to testing would be of interest for predicting the power output of the system. The increase of the power produced per unit volume of the HPEH1-2 compared to HPEH1-1, as seen in table 1, indicates that optimizing the effective area ratio is one aspect of a HPEH system that can allow for the stack volume to decrease while still meeting power output requirements of a system.

The results of the HPEH power tests indicate that the hydraulic pressure energy harvester is a viable option for powering sensor nodes, even at the 55 kPa pressure amplitude level, as low duty cycle sensors can run on as low as 100 μW [35]. The dynamic pressure ripple and the piezoelectric stack voltage time-domain waveforms correspond well, indicating good coupling between the stack and the pressure ripple. The effective area ratio is shown to be an important aspect of the HPEH design, especially in terms of optimizing power produced per unit volume. The spectrum plots of the dynamic pressure and stack voltage indicate that the impedance matching performed for the HPEH for a frequency of 450 Hz is optimal for the hydraulic system used.

6. Model and test comparison

The modeling section provides the groundwork to predict the power output of the HPEH system. Accurate modeling would allow for better optimization of a HPEH for a given hydraulic system and require proper identification of parameters. Tests conducted in the hydraulic system allow $d_{33}^{\text{eff}}F_0$ to be identified, or more specifically $d_{33}^{\text{eff}}A^{\text{eff}}$ as P_0 is known, but cannot individually identify the mechanical force and electromechanical coupling due to the unknown nature of the fluid-mechanical coupling in the HPEH housing. Hence, to identify the d_{33}^{eff} value, and in turn the effective area to find F_0, the piezoelectric sample is removed from the hydraulic system and installed on an experimental rig where an electromechanical shaker is used to excite the stack. Using a force transducer in series with the stack, the electromechanical model based on harmonic excitation, presented earlier, is used to extract a more accurate value of d_{33}^{eff}. Note that this is not the usual d_{33} of the piezoelectric material, since the stack is assembled as a layered configuration of multiple thin layers connected in parallel. Moreover, this identification allows for imperfect force transmission information to be gleaned from tests in the hydraulic system as the force is found from the known pressure input to the system and the experimentally-determined effective area. This technique identified the effective piezoelectric strain term with a 95% confidence level to be 182.93 ± 0.56 nC/N. Using the identified d_{33}^{eff} and measured capacitance values, the method presented in the theory allowed for simulated results of the power output of the HPEH system for a given stack and pressure ripple level and allowed for the effective area due to the fluid-mechanical coupling to be determined. Model results for HPEH1-2 are shown as the model uses the effective areas derived from the determined HPEH1-1 effective area and calculated effective area ratio.

The model for the periodic excitation of a piezoelectric stack is used for the predicted power output (including power normalized by squared force rather than squared pressure ripple amplitude, where force is the product of the pressure amplitude and effective area). The frequency response function $\alpha(\omega)$ was determined via equation (7) and from the test data results of the quotient of the stack voltage over the applied force. All variables for the model for $\alpha(\omega)$ were known, however, in order to compare the model to the actual results, A^{eff} is needed to determine force. Therefore,

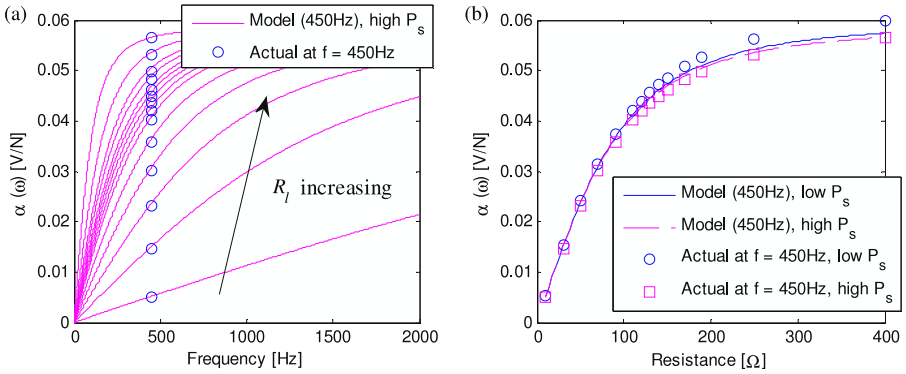

Figure 8. Voltage FRFs (a) versus frequency for a set of resistors (b) versus resistance at 450 Hz (for HPEH1-2).

Table 2. Effective area and effective area ratio for HPEH1-1 and HPEH1-2.

$A^{\text{eff}}_{\text{HPEH1}-1}$	$A^{\text{eff}}_{\text{HPEH1}-2}$	γ_e
$(57.89 \pm 0.91) \times 10^{-6}$ m^2	$(84.13 \pm 6.96) \times 10^{-6}$ m^2	1.45 ± 0.12

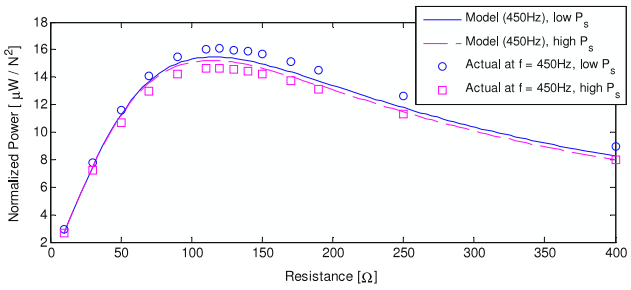

Figure 9. Average normalized power for HPEH1-2 at the peak harmonic of 450 Hz for the low and high static pressure values of 2.07 and 3.45 MPa.

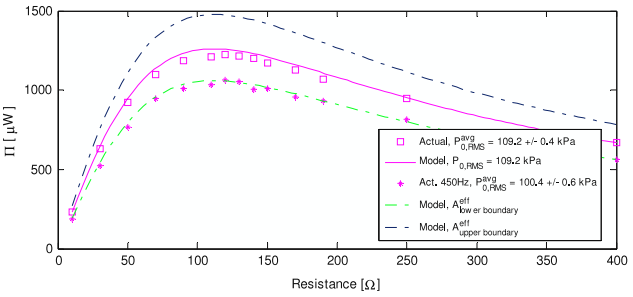

Figure 10. Comparison of the total power harvested and the power harvested at the peak harmonic of 450 Hz for HPEH1-2 at 3.45 MPa (high static pressure).

$A^{\text{eff}}_{\text{HPEH1}-1}$ is found via

$$A^{\text{eff}}_{\text{HPEH1}-1} \cong A_{\text{stack}} \sqrt{\frac{\Pi^{\text{test\_results}}_{\text{HPEH1}-1}}{\Pi^{\text{stack\_area}}_{\text{model}}}} \tag{12}$$

which uses the power from the HPEH1-1 tests, the piezoelectric stack area, and the power calculated from the model using the stack area with all other variables identical to the HPEH1-1 testing parameters. The effective area ratio, γ_e, can be determined by comparing power output and pressure input results from HPEH1-1 and HPEH1-2 tests through

$$\gamma_e = \frac{\sqrt{\Pi_{\text{HPEH1}-2}}}{P_{\text{HPEH1}-2}} \Big/ \frac{\sqrt{\Pi_{\text{HPEH1}-1}}}{P_{\text{HPEH1}-1}}. \tag{13}$$

This then leads to finding an effective area of the HPEH1-2 device by

$$A^{\text{eff}}_{\text{HPEH1}-2} = \gamma_e A^{\text{eff}}_{\text{HPEH1}-1}, \tag{14}$$

which allows for modeling to be performed using the HPEH1-2 device with a predicted effective area. Effective areas and area ratio with standard deviation results are shown in table 2.

Using the calculated $A^{\text{eff}}_{HPEH1-2}$, the model corresponds closely to the experimental results of the system when comparing values at the peak frequency of 450 Hz, as can be seen in figure 8. When considering the different resistance values tested for the different static pressure cases, power output normalized by force input squared is predicted with marginal variability relative to the experimental results, as can be seen in figure 9.

The modeling also compares the total power output across all frequencies with the power output at the peak frequency of 450 Hz, seen in figure 10. The model value is obtained by multiplying the squared average of the test data force inputs of the system by the normalized power output shown previously. This allows for power output predictions of a HPEH device with predetermined parameter values when an excitation force is provided.

From the spectrum of the HPEH system, shown in figure 6, it was observed that most of the energy in the pressure ripple was at 450 Hz. This was also confirmed when comparing the power output from 450 Hz output values to the total power output, as seen in figure 10. The model of the total power output (from all frequencies tested) in comparison to the measured power output shows close

correspondence, allowing for the system power output to be predicted effectively. Note, using the outer limits of the effective area's standard deviation allowance as the effective area in the calculations provide for the power output upper and lower boundary model predictions in figure 10. It can be concluded from these results that the linear modeling assumption holds since the induced electric field level is low (due to parallel connection of the stack layers) and the excitation frequency is well below the resonance frequency of the stack.

7. Conclusion

This paper introduced the concept of low-power electricity generation from pressure ripple in hydraulic systems through piezoelectric stack configurations. Two prototype versions were tested and characterized under different static and dynamic pressure levels. The initial Hydraulic Pressure Energy Harvester (HPEH) prototype provided power outputs of up to 1.2 mW from a dynamic pressure ripple of 400 kPa. The second version of the prototype shows that an effective area ratio greater than unity improves the power output capability of the device. The area ratio and power per unit volume comparison between the device designs tested indicate that optimizing the volume of the piezoelectric stack is of interest. Additionally, a model was presented that was able to couple the hydraulic dynamic pressure ripple to the voltage output of the piezoelectric stack. The simulations show good correlation with the actual results, which can be further used for the power output prediction of systems. Future research involves optimizing effective areas and determining ideal stack characteristics used in HPEH devices to improve the power output to volume ratio of devices.

The results presented here indicate that the high energy density of hydraulic systems is a viable source for off-resonance energy harvesting, from which harvested energy can be used to power a sensor node via the pressure ripple of the hydraulic system.

Acknowledgments

The authors would like to thank Elliott Gruber, Daniel Kim and Nick Earnhart for assistance with experiments concerning the hydraulic pump system and determining the stacks' effective piezoelectric strain constants. This research was supported in part by the Center for Compact and Efficient Fluid Power, a National Science Foundation Engineering Research Center funded under cooperative agreement number EEC-0540834.

References

[1] Beeby S P, Tudor M J and White N M 2006 Energy harvesting vibration sources for microsystems applications *Meas. Sci. Technol.* **17** R175–95

[2] Anton S R and Sodano H A 2007 A review of power harvesting using piezoelectric materials (2003–2006) *Smart Mater. Struct.* **16** R1–21

[3] Priya S 2007 Advances in energy harvesting using low profile piezoelectric transducers *J. Electroceram.* **19** 167–84

[4] Cook-Chennault K A, Thambi N and Sastry A M 2008 Powering MEMS portable devices—a review of non-regenerative and regenerative power supply systems with special emphasis on piezoelectric energy harvesting systems *Smart Mater. Struct.* **17**

[5] Federspiel C C and Chen J 2003 Air-powered sensor *IEEE Sensors (Oct 2003)* **1** 22–5

[6] Priya S, Chen C T, Fye D and Zahnd J 2005 Piezoelectric windmill: a novel solution to remote sensing *Japan. J. Appl. Phys. 2* **44** L104–7

[7] Myers R, Vickers M, Kim H and Priya S 2007 Small scale windmill *Appl. Phys. Lett.* **90** 054106

[8] Xu F J, Yuan F G, Hu J Z and Qiu Y P 2010 Design of a miniature wind turbine for powering wireless sensors *P Soc. Photo-Opt Ins* **7647** 764741

[9] Allen J J and Smits A J 2001 Energy harvesting eel *J. Fluid Struct.* **15** 629–40

[10] Pobering S, Ebermeyer S and Schwesinger N 2009 Generation of electrical energy using short piezoelectric cantilevers in flowing media *Active and Passive Smart Structures and Integrated Systems 2009 (March 2009)* p 728807

[11] Akaydin H D, Elvin N and Andreopoulos Y 2010 Wake of a cylinder: a paradigm for energy harvesting with piezoelectric materials *Exp. Fluids* **49** 291–304

[12] De Marqui C, Erturk A and Inman D J 2010 Piezoaeroelastic modeling and analysis of a generator wing with continuous and segmented electrodes *J. Intell. Mater. Syst. Struct.* **21** 983–93

[13] De Marqui C, Vieira W G R, Erturk A and Inman D J 2011 Modeling and analysis of piezoelectric energy harvesting from aeroelastic vibrations using the doublet-lattice method *J. Vib. Acoust.-Trans. ASME* **133** 011003

[14] Bryant M, Wolff E and Garcia E 2011 Parametric design study of an aeroelastic flutter energy harvester *Proc. SPIE* **7977** 79770S

[15] Bryant M, Fang A and Garcia E 2010 Self-powered smart blade: helicopter blade energy harvesting *P Soc. Photo-Opt Ins* **7643** 764317

[16] Erturk A, Vieira W G R, De Marqui C and Inman D J 2010 On the energy harvesting potential of piezoaeroelastic systems *Appl. Phys. Lett.* **96** 184103

[17] Sousa V C, Anicezio M D, De Marqui C and Erturk A 2011 Enhanced aeroelastic energy harvesting by exploiting combined nonlinearities: theory and experiment *Smart Mater. Struct.* **20** 094007

[18] Peng Z L and Zhu Q 2009 Energy harvesting through flow-induced oscillations of a foil *Phys. Fluids* **21** 123602

[19] St Clair D, Bibo A, Sennakesavababu V R, Daqaq M F and Li G 2010 A scalable concept for micropower generation using flow-induced self-excited oscillations *Appl. Phys. Lett.* **96** 144103

[20] Wang D A and Liu N Z 2011 A shear mode piezoelectric energy harvester based on a pressurized water flow *Sensors Actuators* A **167** 449–58

[21] Deterre M, Lefeuvre E and Dufour-Gergam E 2012 An active piezoelectric energy extraction method for pressure energy harvesting *Smart Mater. Struct.* **21** 85004–12

[22] Elvin N G and Elvin A A 2009 The flutter response of a piezoelectrically damped cantilever pipe *J. Intell. Mater. Syst. Struct.* **20** 2017–26

[23] Tang L S, Paidoussis M P and Jiang J 2009 Cantilevered flexible plates in axial flow: energy transfer and the concept of flutter-mill *J. Sound Vib.* **326** 263–76

[24] Dunnmon J A, Stanton S C, Mann B P and Dowell E H 2011 Power extraction from aeroelastic limit cycle oscillations *J. Fluid Struct.* **27** 1182–98

[25] Kwon S D 2010 A T-shaped piezoelectric cantilever for fluid energy harvesting *Appl. Phys. Lett.* **97** 164102
[26] Giacomello A and Porfiri M 2011 Underwater energy harvesting from a heavy flag hosting ionic polymer metal composites *J. Appl. Phys.* **109** 084903
[27] Humdinger Wind Energy LLC 2013 Windbelt data sheet www.humdingerwind.com
[28] Jung H J and Lee S W 2011 The experimental validation of a new energy harvesting system based on the wake galloping phenomenon *Smart Mater. Struct.* **20** 055022
[29] Zhu D B, Beeby S, Tudor J, White N and Harris N 2010 A novel miniature wind generator for wireless sensing applications *IEEE Sensors (Nov 2010)* 1415–8
[30] Horowitz S B, Sheplak M, Cattafesta L N and Nishida T 2006 A MEMS acoustic energy harvester *J. Micromech. Microeng.* **16** S174–81
[31] Kim S H, Ji C H, Galle P, Herrault F, Wu X S, Lee J H, Choi C A and Allen M G 2009 An electromagnetic energy scavenger from direct airflow *J. Micromech. Microeng.* **19** 094010
[32] Wu L Y, Chen L W and Liu C M 2009 Acoustic energy harvesting using resonant cavity of a sonic crystal *Appl. Phys. Lett.* **95** 013506
[33] Zhao S and Erturk A 2012 Deterministic and stochastic energy harvesting from axial vibrations of a piezoelectric stack *ASME Sensors and Actuators* A submitted
[34] Erturk A and Inman D J 2011 *Piezoelectric Energy Harvesting* (Chichester: Wiley)
[35] Rabaey J A J, Otis B, Burghardt F, Chee Y H, Pletcher N, Sheets M and Qin H 2006 Ultra-low-power design *IEEE Circuits Devices Mag.* **23** 23–9